



UNIVERSITY OF LEEDS

This is a repository copy of *A Framework for Simulation of Magnetic Soft Robots using the Material Point Method*.

White Rose Research Online URL for this paper:

<https://eprints.whiterose.ac.uk/198429/>

Version: Accepted Version

Article:

Davy, J orcid.org/0000-0001-9483-111X, Lloyd, P, Chandler, JH orcid.org/0000-0001-9232-4966 et al. (1 more author) (2023) A Framework for Simulation of Magnetic Soft Robots using the Material Point Method. IEEE Robotics and Automation Letters, 8 (6). pp. 3470-3477. ISSN 2377-3766

<https://doi.org/10.1109/lra.2023.3268016>

This is an author produced version of an article published in IEEE Robotics and Automation Letters, made available under the terms of the Creative Commons Attribution License (CC-BY), which permits unrestricted use, distribution and reproduction in any medium, provided the original work is properly cited.

Reuse

This article is distributed under the terms of the Creative Commons Attribution (CC BY) licence. This licence allows you to distribute, remix, tweak, and build upon the work, even commercially, as long as you credit the authors for the original work. More information and the full terms of the licence here:

<https://creativecommons.org/licenses/>

Takedown

If you consider content in White Rose Research Online to be in breach of UK law, please notify us by emailing eprints@whiterose.ac.uk including the URL of the record and the reason for the withdrawal request.



eprints@whiterose.ac.uk
<https://eprints.whiterose.ac.uk/>

A Framework for Simulation of Magnetic Soft Robots using the Material Point Method

Joshua Davy, Peter Lloyd, James H. Chandler *Member, IEEE* and Pietro Valdastri *Fellow, IEEE*

Abstract—Simulation represents a key aspect in the development of robot systems. The ability to simulate behavior of real-world robots provides an environment where robot designs can be developed and control systems optimized. Due to the use of external magnetic fields for actuation, magnetic soft robots can be wirelessly controlled and are easily miniaturized. However, the relationship between magnetic soft materials and external sources of magnetic fields present significant complexities in modelling due to the relationship between material elasticity and magnetic wrench (forces and torques). In this work, we present a simulation framework for magnetic soft robots using the Material Point Method (MPM) which integrates hyper-elastic material models with the magnetic wrench induced under external fields. Compared to existing Finite Element Methods (FEM), the presented MPM based framework inherently models self-collision between areas of the model and can capture the effect of forces in non-homogeneous magnetic fields. We demonstrate the ability of the MPM framework to model the influence of magnetic wrench on magnetic soft robots, capture dynamic behavior of robots under time-varying magnetic fields, and provide an accurate representation of deformation when colliding with obstacles. We show the versatility of MPM framework by comparing simulations to a range of real-world magnetic soft robot designs previously presented in the literature.

Index Terms—Modeling, Control, and Learning for Soft Robots; Soft Robot Materials and Design; Simulation and Animation

I. INTRODUCTION

MAGNETIC soft robots (MSRs) are of interest due to the potential for miniaturization afforded by off-board actuation [1][2][3][4][5]. By manipulating this magnetic field, the resultant wrench (forces and torques) on magnetic segments of the robot can be precisely controlled. This makes MSRs well suited to applications in surgery where the soft

structure of the robot and small scale can enable them to reach areas of the anatomy unachievable by conventional tooling [6][7]. MSRs can be formed by embedding permanent magnets or magnetic microparticles into soft elastomeric materials [8][9]. The latter case is appealing due to the ability to retain an entirely soft structure. However, this scenario presents a challenging system to model with standard approaches due to material geometry, direction of magnetization, external magnetic field and external forces all influencing the resultant deformation.

Finite element methods (FEM) have been used to model MSRs and represent a high accuracy approach capable of modeling hyper-elastic deformation under external fields while representing complex geometries [10][11]. MSRs, make use of *hard magnetic* materials which are defined by their remnant magnetization once an external magnetizing field is removed. In order to simplify the FEM modeling of MSRs, the assumption of discrete hard magnetic elements embedded within the soft material can be made [12][13]. However, this assumption is only valid on MSRs formed with discrete magnetic sections, and loses accuracy as the deformation of these sections increases [14]. Zhao et al. [11] addressed this significant problem by deriving a stress relationship for magnetically hard, mechanically soft materials and integrated it into FEM software (ABAQUS, Dassault Systèmes, France) allowing continuous, deformable magnetic profiles within the material [11]. By the combination of hyper-elastic models with the magnetic contribution of stress in the material, they demonstrate the accurate prediction of equilibrium deformation under constant fields. Nonlinear FEM analysis comes at significant computational cost due to the numerical iterative minimization process. Furthermore, under large hyper-elastic deformation the mesh representation utilized in FEM can become distorted, leading to erroneous results and poor convergence [15]. Ye et al. presented Magttice, a FEM-based lattice model by integrating the magnetic potential energy derived by Zhao et al. into a lattice mesh model [10]. They proceed to study the interaction between MSRs with fluids in time varying fields, noting the importance of considering gravity into the model to provide accurate deformation results.

As an alternative approach to FEM, the Material Point Method (MPM) is a hybrid Lagrangian, Eulerian model for continuum mechanics [16][17]. Unlike FEM, there is no underlying deforming mesh in the model. Instead MPM is a cyclical process which moves between a particle based representation and a fixed grid. The particle representation is utilized for internal material stress and the grid provides a structure to apply external forces. The lack of deforming mesh prevents

Manuscript received: October, 31, 2022; Revised March, 16, 2023; Accepted April, 11, 2023.

This paper was recommended for publication by Editor Jessica Burgner-Kahrs upon evaluation of the Associate Editor and Reviewers' comments.

Research reported in this article was supported by the Engineering and Physical Sciences Research Council (EPSRC) under grants number EP/R045291/1 and EP/V009818/1, and by the European Research Council (ERC) under the European Union's Horizon 2020 research and innovation programme (grant agreement No 818045). Any opinions, findings and conclusions, or recommendations expressed in this article are those of the authors and do not necessarily reflect the views of the EPSRC or the ERC.

For the purpose of open access, the authors have applied a Creative Commons Attribution (CCBY) license to any Accepted Manuscript version arising.

Joshua Davy, Peter Lloyd, James H. Chandler, and Pietro Valdastri are with the STORM Lab, Institute of Autonomous Systems and Sensing (IRASS), School of Electronic and Electrical Engineering, University of Leeds, Leeds, UK. Email: {e117jd, men9pr1, j.h.chandler, p.valdastri}@leeds.ac.uk

Digital Object Identifier (DOI): see top of this page.

the issue of mesh collapse under high deformation experienced in FEM. Unlike FEM, the use of discrete material points can implicitly handle self-collision and model fracturing and has found application in crack propagation of beams and the study of tissue-needle interaction [18][19]. The nature of this method suits the mass parallelization of processing across multiple processors, as individual updates of particle and grid nodes can be considered independently and the effects summated. Further, due to the continuous nature of MPM, derivatives of the current state with respect to the initial model parameters can be obtained and utilized to guide optimization to achieve desired behaviour [17].

In this work, we extend the MPM to cover magnetically hard, mechanically soft materials. Using this approach, we demonstrate the ability to model large deformations in MSRs under varying fields. Our system is capable of representing dynamic behavior and collisions in the environment, as well as the final equilibrium state in static fields. Additionally, as the MPM representation associates each particle with its own magnetization vector, MSRs can be modeled with varied and near continuous magnetization profiles. Thus, our methodology and simulation environment is capable of representing complex MSR scenarios and capturing their resultant behavior.

In an extension to previously presented FEM modeling, we showcase the ability to model not just torques but also magnetic forces present caused by non-homogeneous magnetic fields. Unlike FEM approaches, self collision between model parts is implicit in the MPM allowing the physical interaction between segments of the robot to be studied. We further show how the MPM methodology means external forces can be easily integrated into the model providing realistic interactions with surfaces and obstacles.

We validate these models on fabricated MSRs and show agreement with the derived MPM model. We further showcase robot designs from the literature in the simulation framework and replicate behaviours as observed in reality. Open source examples of 3D implementation of the framework are available at <http://github.com/joshdavy1/magneticMPM>.

II. A REVIEW OF THE MATERIAL POINT METHOD.

MPM is an Eulerian-Lagrangian numerical method for continuum mechanics consisting of two material representations. The first, the Lagrangian representation consists of individual particles of a fixed mass and volume that represent discretized elements of the material. These elements are initially distributed evenly to represent the geometry of the material. The second is the grid representation, which can be considered as an undeformable Eulerian mesh, which is fixed in reference frame. This grid consists of regular node points, surrounding the material. The grid nodes are static in position and regularly spaced but represent a transfer of particle properties from one time-step to the next.

Transfers between representations are named Particle-to-Grid (P2G) (Fig. 1a) and Grid-to-Particle (G2P) (Fig. 1c), respectively. Our work extends the Moving Least Squares - Material Point Method (MLS-MPM) algorithm in order to represent the actuation experienced in magnetic materials [20].

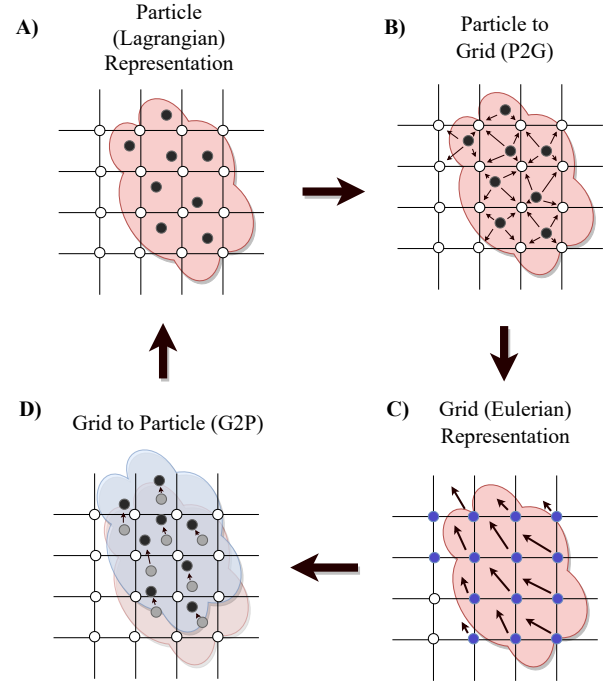


Fig. 1: The cyclical method followed by MPM. a) Internal forces and magnetic stress are computed in the particle domain. b) Particle properties are transferred to grid representation. c) External interaction and forces due to magnetic gradients are computed in the grid domain. d) Particle properties are reconstructed from the grid.

The following gives an overview of the MLS-MPM; readers are referred to the works of [20] and [21] for an extensive overview and full derivations.

A. Particle (Lagrangian) Representation

Particles are initialized in order to represent the geometry of the soft robot and their position at time t is notated as $\mathbf{x}_p^t \in \mathbb{R}^3$. $\mathbf{v}_p^t \in \mathbb{R}^3$ represents the particle velocity vector and $\mathbf{C}_p^t \in \mathbb{R}^{3 \times 3}$ represents the affine velocity matrix [22]. A final variable $\mathbf{F}_p^t \in \mathbb{R}^{3 \times 3}$ represents the particle deformation gradient initialized to the identity matrix $\mathbf{F}_p^0 = \mathbb{I}$.

B. Particle to Grid (P2G)

In order to transfer the particle representation of the material to the grid, we must distribute the properties of the particle to the surrounding nodes (see Fig. 1b). To do this, a weighting function is utilized to specify the relative distribution of the particle property to the neighborhood nodes. Here, the properties are distributed using a quadratic B-spline kernel distributed to a $3 \times 3 \times 3$ neighborhood of grid nodes given as

$$W(\Delta \mathbf{r}) = w(\Delta x)w(\Delta y)w(\Delta z) \quad (1)$$

where

$$w(\alpha) = \begin{cases} 0.75 - |\alpha/\delta x|^2 & 0 \leq |\alpha/\delta x| < 0.5 \\ 0.5(1.5 - |\alpha/\delta x|)^2 & 0.5 \leq |\alpha/\delta x| < 1.5 \\ 0 & 1.5 \leq |\alpha/\delta x| \end{cases} \quad (2)$$

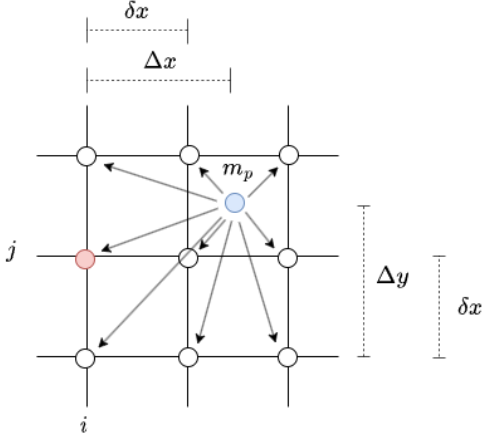


Fig. 2: 2D illustration of the distribution of particle (blue) properties in the P2G step to the node i, j (red) utilising the Quadratic B-spline kernel [21].

[21]. Where $\Delta \mathbf{r} = [\Delta x, \Delta y, \Delta z]^T$ is the relative displacement between particle and the node at i, j, k as shown in Fig. 2. δx is the grid node spacing (See Fig. 2). $\alpha \in \{\Delta x, \Delta y, \Delta z\}$.

As such grid mass is distributed as

$$m_{i,j,k}^t = \sum_p W(\Delta \mathbf{r}) m_p, \quad (3)$$

where m_p is the particle mass equal to ρv_p where ρ is the material density and v_p is the particle volume. Grid momentum is calculated as

$$\mathbf{p}_{i,j,k}^t = \sum_p W(\Delta \mathbf{r}) (m_p \mathbf{v}_p^t - (\frac{4}{\delta x^2} v_p \mathbf{P}_p^t (\mathbf{F}_p^t)^T + m_p \mathbf{C}_p^n) \Delta \mathbf{r}). \quad (4)$$

where \mathbf{P}_p^t is the first Piola–Kirchhoff stress tensor [21].

C. Grid (Eulerian) Representation

After transfer to the grid representation, the effect of external forces are imposed (Fig. 1c). These external forces and the grid momentum can be integrated to form the grid velocity.

$$\mathbf{v}_{i,j,k}^t = \frac{1}{m_{i,j,k}^t} (\mathbf{p}_{i,j,k}^t + \mathbf{f}_{i,j,k}^t \Delta t), \quad (5)$$

where Δt is the simulation time stepping and $\mathbf{f}_{i,j,k}^t$ is the external force on the node. For all nodes where $m_{i,j,k}^t \neq 0$.

D. Grid to Particle (G2P)

After the velocities in the grid frame have been calculated, particle velocity and affine velocity can then be reconstructed utilizing the same weighting kernel specified in Section II-B (Fig. 1d).

$$\mathbf{v}_p^{t+1} = \sum_i \sum_j \sum_k W(\Delta \mathbf{r}) \mathbf{v}_{i,j,k}^t, \quad (6)$$

$$\mathbf{C}_p^{t+1} = \frac{4}{\delta x^2} \sum_i \sum_j \sum_k W(\Delta \mathbf{r}) \mathbf{v}_{i,j,k}^t \Delta \mathbf{r}. \quad (7)$$

The deformation gradient of the particle and particle positions are updated, representing the overall change in deformation and pose of material in the time-step.

$$\mathbf{F}_p^{t+1} = (\mathbb{I} + \mathbf{C}_p^{t+1} \Delta t) \mathbf{F}_p^t \quad (8)$$

$$\mathbf{x}_p^{t+1} = \mathbf{x}_p^t + \mathbf{v}_p^{t+1} \Delta t \quad (9)$$

III. MODELLING OF MAGNETICALLY HARD, MECHANICALLY SOFT MATERIALS.

We consider the modeling of elastomers embedded with magnetic elements, common in soft robotics. Typically, this consists of a silicone prepolymer mixed with hard magnetic microparticles (commonly NdFeB due to its high remnant magnetization). This mixture is then cast into molds of the desired form of the magnetic robot and set [23]. The cast is then subjected to a saturating magnetizing field in order to set the direction of magnetization. After being removed from the field, the material retains a remnant magnetization.

In this work we consider this material as an *ideal hard-magnetic soft material* [11]. The self-interaction between the magnetic elements of the MSR is neglected. This has shown to be a valid assumption for modelling deformation of the MSR due to the relative weakness of this interaction compared to the interaction with larger external magnetic fields [10][23].

A. Elastomeric Properties

For modelling the elastic properties of the material the Neo-Hookean elastic model is adopted which has been shown to accurately model the stress-strain relationship of magnetic soft materials in the strain ranges experienced in soft robotic applications [24]. The Neo-Hookean model is given as

$$\mathbf{P}_{p,elastic}^t = G J^{-2/3} (\mathbf{F}_p^t - \frac{I_1}{3} \mathbf{F}_p^{-T}) + K J (J - 1) \mathbf{F}_p^{-T}. \quad (10)$$

where $\mathbf{P}_{p,elastic}^t$ is the elastic contribution of the first Piola–Kirchhoff stress tensor, G is the shear modulus of the material and K is the bulk modulus. $J = \text{determinant}(\mathbf{F}_p^t)$ and $I_1 = \text{trace}(\mathbf{F}_p^{tT} \mathbf{F}_p^t)$. In order to satisfy the assumption of near incompressibility of the utilized silicone polymers we chose the bulk modulus to be a sufficiently high value. In this case we set $K = 20G$. At the strain/scale ranges relevant to our MSRs, the actual value of the bulk modulus does not largely affect the final deformation [10][11].

B. Magnetic Properties

A magnetic agent under external magnetic fields will experience an aligning torque between the magnetic moment and the external field.

$$\boldsymbol{\tau} = \mathbf{m} \times \mathbf{B} \quad (11)$$

where \mathbf{B} is the external magnetic field and \mathbf{m} is the magnetic moment vector equal to $\frac{\mathbf{B}_r V}{\mu_o}$ where V is the volume of the

agent. μ_0 is the vacuum permeability equal to $4\pi \times 10^{-7} \text{ Hm}^{-1}$ and \mathbf{B}_r is the remnant magnetization vector.

Further, in the case of a non-homogeneous magnetic field, the agent will experience a force,

$$\mathbf{f} = \nabla(\mathbf{B} \cdot \mathbf{m}). \quad (12)$$

This force is proportional to the spatial gradient of the magnetic field and is at maximum with alignment of the magnetic moment and external field.

In the FEM approach outlined by Zhao et al. [11] the effect of aligning torque under homogeneous magnetic fields is integrated into the elastic model via an additional stress. We utilise this stress along with the Neo-hookean model into the P2G step of the MPM cycle. This, in the first Piola-Kirchoff form is

$$\mathbf{P}_p^t{}^{magnetic} = -\frac{1}{\mu_0} \mathbf{B} \otimes \mathbf{B}_{r_p}, \quad (13)$$

where \otimes is the dyadic product and \mathbf{B}_{r_p} is the remnant magnetic flux density associated with the particle. Leading to an overall material stress as

$$\mathbf{P}_p^t = \mathbf{P}_p^t{}^{elastic} + \mathbf{P}_p^t{}^{magnetic}. \quad (14)$$

By incorporating the magnetic stress effect into the P2G, step, the effect of the realigning torque can be incorporated into the MPM. However, the forces induced in non-homogeneous magnetic fields are not covered. Therefore the magnetic force is incorporated as an external force in the grid velocity calculation. To calculate the force at the grid node, we calculate the equivalent magnetic moment of the node as a product of the volume of magnetic particles using the same weightings as described in the P2G Section II-B.

$$\mathbf{m}_{i,j,k}^t = \frac{v_p}{\mu_0} \sum_p W(\Delta \mathbf{r}) \tilde{\mathbf{B}}_{r_p}. \quad (15)$$

where $\tilde{\mathbf{B}}_{r_p}$ is the remnant magnetic flux density rotated into the current reference frame equal to $\frac{1}{J} \mathbf{F}_p^t \mathbf{B}_{r_p}$.

The external magnetic force can then be derived as

$$\mathbf{f}_{magnetic} = \nabla \mathbf{B}_{i,j,k}^T \cdot \mathbf{m}_{i,j,k}^t, \quad (16)$$

where $\nabla \mathbf{B}_{i,j,k}$ is the spatial gradient of the magnetic field at the node.

C. Material Damping

Damping is the energy dissipation of the material and represents numerous complex phenomena (viscosity, air resistance, heat exchange etc.). To capture these properties of magnetic soft materials, we model damping by adding a force proportional to the current grid momentum,

$$\mathbf{f}_{damping} = -c \mathbf{p}_{i,j,k}^t \quad (17)$$

where c is the damping constant. This external force will lead the material to a final equilibrium pose given a static applied field.

Therefore the full set of external forces introduced to the grid operations step is

$$\mathbf{f}_{i,j,k}^t = \mathbf{f}_{magnetic} + \mathbf{f}_{damping} + \mathbf{f}_{gravity} \quad (18)$$

$$\mathbf{f}_{i,j,k}^t = \nabla \mathbf{B}_{i,j,k}^T \cdot \mathbf{m}_{i,j,k}^t - c \mathbf{p}_{i,j,k}^t + m_{i,j,k}^t \mathbf{g} \quad (19)$$

where \mathbf{g} is the acceleration due to gravity.

It is worth noting that the proposed extension of MPM to model magnetic soft materials requires three readily obtained material parameters. These are the material density, the magnetic remanence, and the shear modulus of the material. However, the damping constant is more difficult to obtain. In magnetics, the interest is often in the final equilibrium state of the robot, and therefore a damping parameter leading to a fast settle time of the system is most appropriate. This can be obtained through iterative experimentation. In the case where accurate representation of dynamics is required a methodology such as followed by Shariati et al. may be utilized [25].

IV. EXPERIMENTAL VERIFICATION

A. Implementation

The above stated magnetic MPM algorithm was implemented in the Taichi programming language [26]. Taichi was selected due to supporting GPU parallelization and Python-esque syntax. All examples were run on an NVIDIA Quadro RTX 4000 GPU.

The choice of time-step significantly affects the speed of simulation and a maximum time-stepping should be chosen that retains model stability. As derived in [27], the maximum time stepping for MPM is

$$\Delta t_{max} = C \delta x \sqrt{\frac{\rho}{3G}} \quad (20)$$

where C is a constant close to one. It is evident that the time-stepping can be increased by utilising large grid node spacing. However, this limits the fidelity in which external forces can be incorporated. A balance must be found between grid node spacing and simulation speed. It can also be observed from (20) that the stiffer, less dense materials lead to a lower maximum time-stepping. The number of particles N , further effects the simulation performance. Low particle numbers fail to fully represent the deformation of the robot, while high numbers will add significant computation time. The generation of the initial pose of the particles is performed by uniformly distributing particles in the geometry of the structure. This is performed via sampling 3D models of the robot. We first validate our methodology empirically on planar models; verifying agreement with real world behaviour. We then present a full 3D implementation of the magnetic MPM framework and showcase simulations of MSRs from the literature. All material parameters were obtained following the methodology of [24].

B. Magnetic Beam Deformation

To validate the approach, we recreate the high deformation beam bending experiment presented by Zhao et al. [11]. A magnetically hard materially soft beam ($G = 303 \text{ kPa}$, $|\mathbf{B}_r| = 0.258 \text{ T}$) manufactured from PDMS (Sylgard 184) is placed in a external magnetic field. The direction of applied field is

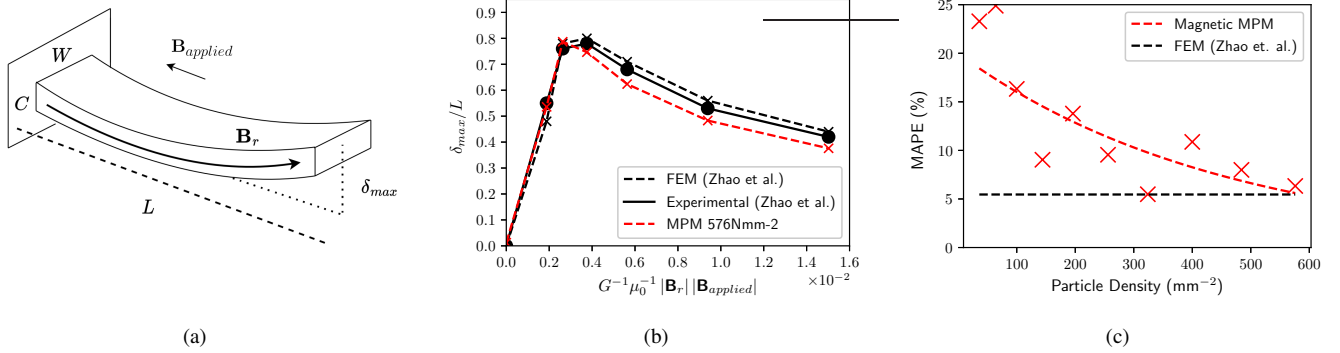


Fig. 3: High deformation magnetic soft beam experiment as presented by Zhao et al [11]. (a) The applied field $\mathbf{B}_{\text{applied}}$ is in the opposite direction to the remnant magnetization \mathbf{B}_r of the soft material leading to high deflection. ($L = 17.2$ mm, $C = 0.84$ mm, $W = 5$ mm). (b) Magnetic MPM methodology compared with experimental results and FEM analysis [11] $G^{-1}\mu_0^{-1}|\mathbf{B}_r||\mathbf{B}_{\text{applied}}|$ is a constant which leads these results to be independent of material parameters. (c) Mean Absolute Percentage Error (MAPE) converges with increased particle density.

parallel yet opposite to the remnant magnetization vector of the beam (See Fig. 3a); causing a deflection under increasing field strength. We recreate this scenario in our framework with a varying particle density to represent the beam ($\delta x = 0.3$ mm, $\Delta t = 6 \times 10^{-6}$ s). We then compare the resultant deflection δ_{max}/L with the experimental data and FEM results provided by the authors (See Fig. 3b). Fig. 3c shows how the results converge with particle density leading to a 6.1% Mean Absolute Percentage Error (MAPE) with a particle density of 576 mm^{-2} . This data informed choices on particle density in the following experiments.

C. Deformation under Non-homogeneous Magnetic Fields.

To verify the ability of the MPM framework to model forces experienced due to magnetic field gradients the interaction between a permanent magnet and a MSR is studied. The robot was magnetized along its main axis and placed vertically above a $100 \text{ mm} \times 100 \text{ mm}$ cylindrical neodymium magnet with a remanence of 1.44 T (See Fig. 4). The MSR is fabricated from Ecoflex-30 silicone polymer (Smooth-On, Inc., U.S.A.)

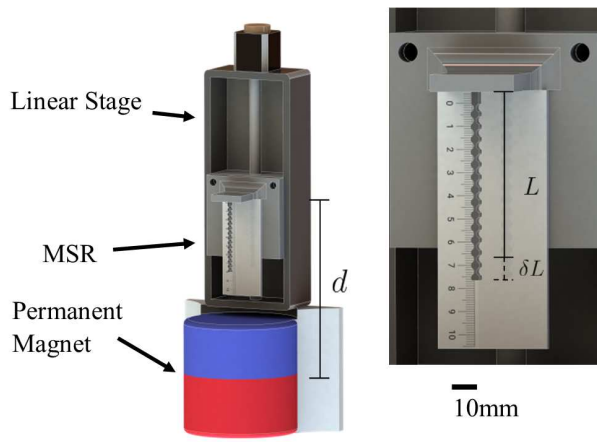


Fig. 4: Experimental setup for measuring the deformation of the MSR due to gradient forces. A linear stage moves the robot closer to the permanent magnet where gradient forces are stronger. This causes an extension of length in the MSR.

mixed with NdFeB microparticles in a 1:1 mass ratio ($G = 33$ kPa, $|\mathbf{B}_r| = 0.101 \text{ T}$, $\rho = 1840 \text{ kgm}^{-3}$). In this configuration, no magnetic torques are present due to the alignment of the robot's magnetization with the permanent magnet. The design of the MSR has periodic thickness in order to give an exaggerated deformation compared to a simple beam. Thicker sections increase the overall magnetic moment whilst thinner sections give larger strain due to lower elastic forces. The MSR is mounted to a linear stage allowing the introduction of the robot towards the magnet. As the robot is moved towards the magnet, larger magnetic fields gradients are present which causes an extension of robot length. This strain is compared to the same experimental setup in simulation ($\delta x = 2$ mm, $\Delta t = 1 \times 10^{-6}$ s, $N = 15, 359$). A model of the magnetic field from a cylindrical permanent magnet is provided by Magpylib [28] and finite differences are used to obtain the spatial gradient of the magnetic field.

Fig. 5 shows the results from simulation and experimental setup. Due to the alignment of the magnetic field and magnetization of the robot, the gradient effect can be independently observed. The results are in strong agreement and the error at lower distances to the magnet can be attributed to limitations in magnetic field modelling and accuracy of hyper-elastic model rather than an inherent fault in methodology.

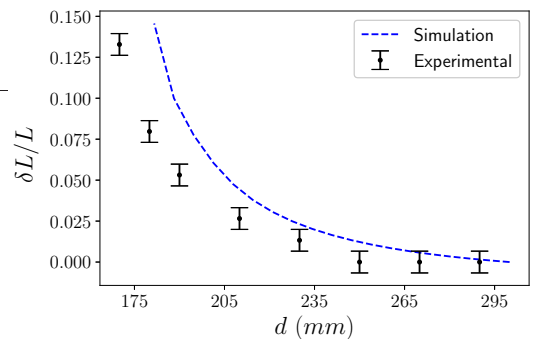


Fig. 5: Comparison of simulation and experimental results for the deformation of the robot as described in Section IV-C due to increasing field gradient forces as its introduced towards the magnet.

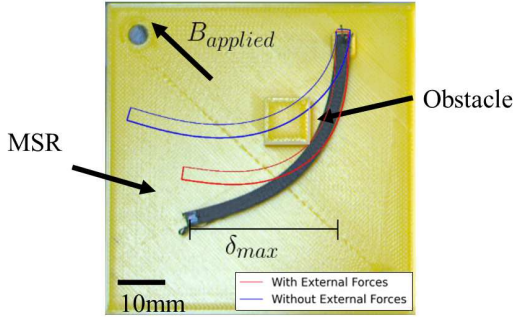


Fig. 6: Experimental setup measuring deformation when interacting with external obstacles. Red and blue outlines represent the resultant deformation under the applied magnetic field, considering and not considering the interaction with the obstacle respectively. $|\mathbf{B}_{applied}| = 10$ mT.

D. Interaction with External Bodies.

The MPM implicitly handles self-collision between material points. This is a significant advantage over FEM methods which require additional interpolation between mesh vertices to handle this self collision. In the MPM framework, external forces can be integrated into the model in the grid representation. To demonstrate the ability to model interaction with external entities we consider the deformation of an axially magnetized MSR under contact with a rigid obstacle. This is represented in the grid representation stage by setting the grid velocity to zero at the obstacle boundary on collision with the obstacle,

$$\mathbf{v}_{out} = \begin{cases} \mathbf{0} & \text{if } \mathbf{v}_{in\parallel} \geq 0, \\ \mathbf{v}_{in} & \text{otherwise.} \end{cases} \quad (21)$$

where \mathbf{v}_{in} is the incoming velocity calculated in Equation (5) and \mathbf{v}_{out} is the velocity used in particle property reconstruction in section II-D. \parallel represents the parallel component of the velocity vector between the obstacle and the MSR.

A MSR of dimensions 60x3x3 mm is fabricated from Dragonskin-10 silicone polymer (Smooth-On, Inc., U.S.A.) mixed with NdFeB microparticles in a 1:1 mass ratio, ($G = 120$ kPa, $|\mathbf{B}_r| = 0.125$ T, $\rho = 1882$ kgm⁻³) [24]. The MSR is axially magnetized and deflected via an applied magnetic field from a resting state under gravity to collide with a plastic obstacle (See Fig. 6). Fig. 7 shows normalized maximum deflection δ_{max}/L with increasing applied magnetic field, when considering the external object in the MPM framework. At large deflection, a larger difference in tip position can be noted. This can be attributed to the accuracy of the underlying hyper-elastic model (Equation (10) at high deformation.

E. Magnetic Soft Robots from the Literature.

MSRs vary from the sub-millimeter to larger centimeter-scale [2][6][23][29]. In this section, we showcase the utility of our MPM-framework by replicating designs of MSRs as presented in the literature.

1) *Continuum MSR (Pittiglio et al [23]):* We first consider the continuum MSR presented by Pittiglio et al. [23]. These robots are formed of alternating magnetic and non-magnetic

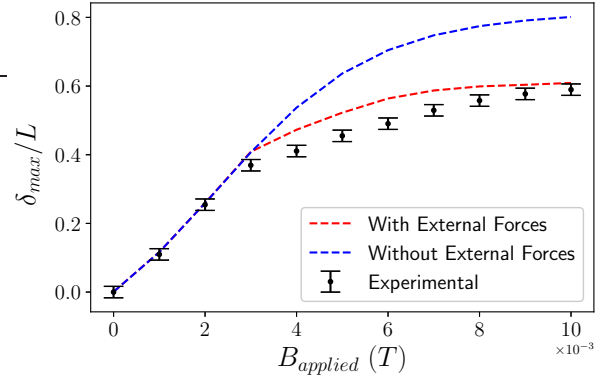
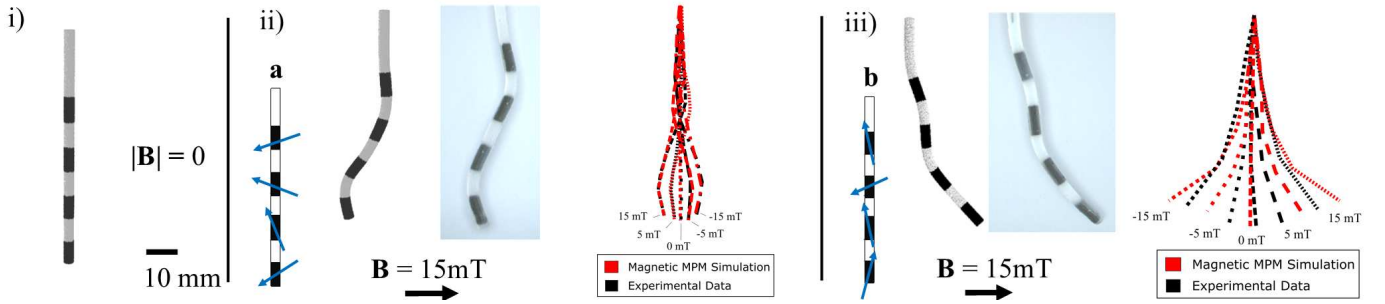


Fig. 7: Comparison of maximum normalized deflection δ_{max}/L of the MSR with experimental results when external interaction is considered. ($\delta x = 2$ mm, $\Delta t = 5 \times 10^{-5}$ s, $N = 11,520$)

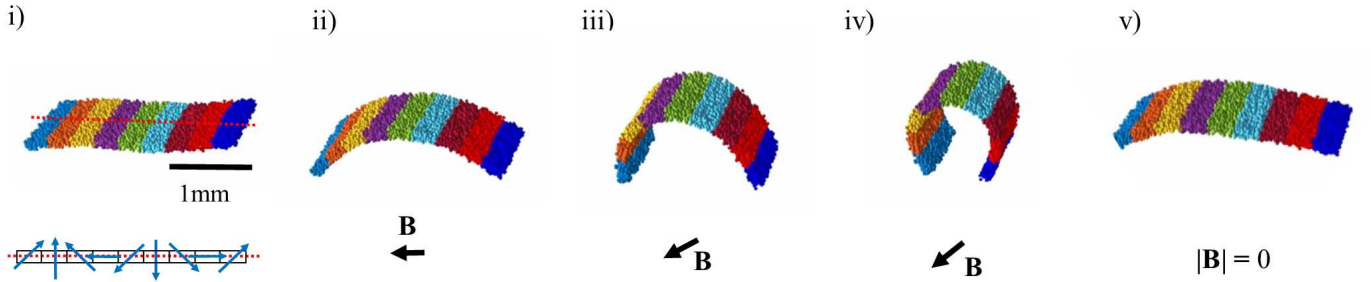
sections. The direction of the magnetization vector of each section is decided by an optimization algorithm to give a desired shape under a given magnetic field. We reproduce the continuum MSR in simulation and applied the same magnetic profile as presented ($\delta x = 1$ mm, $\Delta t = 2 \times 10^{-5}$ s, $c = 200$ s⁻¹, $N = 118,271$) with two magnetization profiles (**a** and **b**). Material parameters were obtained from the work, and a damping parameter was chosen to provide fast equilibrium of the system. In Fig. 8a it can be observed that under the same magnetic field with matching profiles, the simulation and real robot produce deformations closely matching the real world behaviour. (See Supplementary Video).

2) *Small scale soft robot (Hu et al. [29]):* We reproduce the MSR designed by Hu et al. [29] in our framework and make use of the collision model of Equation (21) to represent a floor with which the robot can interact ($\delta x = 0.1$ mm, $\Delta t = 7 \times 10^{-7}$ s, $c = 180$ s⁻¹, $N = 10,260$). The robot presented by the authors is formed of a continuous magnetic profile along its length; we represent this as a series of nine sections with a matching magnetic profile (See Fig. 8b). By applying a rotating external magnetic field of varying magnitude, the 'walking' behavior observed by the authors is recreated. The ability to replicate this complex behaviour in simulation shows the potential of the MPM framework to iteratively design and test MSRs when compared to complex fabrication and experimental setups in reality. (See Supplementary Video).

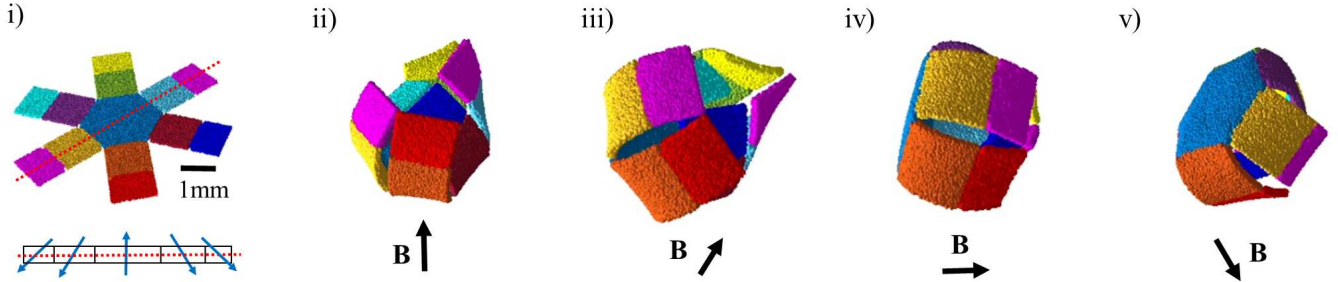
3) *Six armed untethered gripper (Xu et al. [13]):* The final example taken from the literature is the six-armed untethered gripper robot presented by Xu et al. [13]. This robot consists of 13 magnetic sections each with its own magnetization vector. On the application of a magnetic field perpendicular to the undeformed robot, the robot folds up and is capable of grasping small objects. The direction of magnetic field can be rotated and the robot will then roll in the direction of rotating field of angular frequency $\omega = 10$ Hz. This behavior is recreated in Fig. 8c and shown in the Supplementary Video. ($\delta x = 0.1$ mm, $\Delta t = 5 \times 10^{-7}$ s, $c = 20$ s⁻¹, $N = 103,430$). The grasping behaviour of the robot is a product of the self-collision between the robot's arms. This behavior is inherent in the MPM algorithm unlike FEM approaches which require



(a) Simulation of continuum MSR developed by Pittiglio *et al.* [23]. i) MSR under no external field. ii) Deformation under field in simulation with magnetization profile **a** (left), deformation under field in experimental setup with fabricated MSR (center) and transient behaviour under magnetic field sweep (right). Mean tip positional error across sweep = 0.38 mm. iii) Deformation under field in simulation with magnetization profile **b** (left) and deformation under field in experimental setup with fabricated MSR. (center) and transient behaviour under magnetic field sweep (right). Mean tip positional error across sweep = 6.97 mm. MSR length = 80 mm.



(b) The small scale soft robot presented by Hu *et al.* [29], in the presented simulation framework, demonstrating the 'walking' behaviour discussed in the author's work as the magnetic field is rotated. i) Magnetization profile $|B_{max}| = 8$ mT.



(c) The six arm untethered gripper presented by Xu *et al.* [13]. Applying a magnetic field perpendicular to the robot causes it to grasp shut. Once shut, rotating the magnetic field causes the robot to roll. The self-collision between model parts is inherent in our methodology. i) Magnetization profile. $|B| = 15$ mT, $\omega = 10$ Hz.

Fig. 8: MSRs from the literature represented in the MPM framework.

additional computation to interpolate meshes and calculate these interaction forces. (See Supplementary Video).

V. CONCLUSION

In this work, we have presented a novel methodology for simulating MSRs. The Material Point Method (MPM) is capable of accurately representing the deformation experienced in magnetic soft materials at high deformation in the presence of external magnetic fields. Unlike FEM approaches, MPM implicitly represents self-collisions in the material, allowing MSRs that rely on self-interaction to be represented. Further, our methodology has extended what was capable with existing systems by integrating the magnetic forces experienced in non-homogeneous magnetic fields. We have validated the methodology and show strong agreement (6.1% MAPE, Fig 3c) with

real-world deformation at large strains. Further, comparison with MSRs from the literature showcases the ability of the presented methodology to replicate the complex behaviour seen in the real robots in simulation.

Existing simulation frameworks for MSRs have often relied on proprietary, closed-source or unreleased implementations. We have made implementation examples of our magnetic MPM framework available in order to allow others to utilize our methodology. Robots can be generated from 3D CAD models with specification of the magnetic profile of each section. The ability to test ideas quickly in simulation (when compared to fabrication and experimental setups), allows the fast iterative design of MSRs. When paired with the ability to model external forces and obstacles, designs can be explored and modified, and complex behaviors can be tested. By releas-

ing our implementation, we hope others developing simulation frameworks can provide direct comparisons with our work.

Our framework is well suited to use as an environment for optimization or training machine learning systems, which can then be applied in reality. For example, the continuum MSR of Pittiglio et. al. [23] were optimized using simplified rigid-link models. Utilising more accurate modelling would allow these designs to closer match the desired objective or incorporate dynamic behaviour under the influence of transient magnetic fields. The mass parallelization of our implementation, leads to efficient run-times by utilising GPU processing.

Unlike FEM, the MPM is a continuous function of the initial variable values. This fact was exploited by Hu et al. [17], to develop a fully differentiable physics simulation to reduce the number of iterations for convergence of design optimization. This could be replicated with our methodology to optimize parameters such as magnetic profile, robot geometry and applied field efficiently.

The presented methodology only considers the interaction between the material's magnetic field and the externally applied actuating field. This neglects any self-interaction between discrete magnetic robot segments. This assumption is suitable for the cases in our experimental verification but, for other MSR designs that may rely on this interaction, their behaviour may not be accurately. An example of this could be the interactive forces between multiple MSRs in the same workspace [27]. Future work could consider the field generated by individual magnetic segments in order to better represent this characteristic. This would, of course, add significant algorithmic and computational complexity to the simulation.

The inherent ability to represent collision between particles in MPM could be utilized to consider the interaction between MSRs and external soft bodies. This is of particular interest due to the clinical applications of MSRs, in order to study the interaction between robots and soft tissues.

REFERENCES

- [1] Y. Kim and X. Zhao, "Magnetic soft materials and robots," *Chemical Reviews*, vol. 122, no. 5, pp. 5317–5364, 2022.
- [2] M. Sitti, "Miniature soft robots—road to the clinic," *Nature Reviews Materials*, vol. 3, no. 6, pp. 74–75, 2018.
- [3] D. Liu, X. Liu, Z. Chen, Z. Zuo, X. Tang, Q. Huang, and T. Arai, "Magnetically driven soft continuum microrobot for intravascular operations in microscale," *Cyborg and Bionic Systems*, vol. 2022, 2022.
- [4] J. Lu, Y. Liu, W. Huang, K. Bi, Y. Zhu, and Q. Fan, "Robust control strategy of gradient magnetic drive for microrobots based on extended state observer," *Cyborg and Bionic Systems*, 2022.
- [5] C. Huang, Z. Lai, X. Wu, and T. Xu, "Multimodal locomotion and cargo transportation of magnetically actuated quadruped soft microrobots," *Cyborg and Bionic Systems*, vol. 2022, p. 0004, 2022.
- [6] E. Diller and M. Sitti, "Micro-scale mobile robotics," *Foundations and Trends® in Robotics*, vol. 2, no. 3, pp. 143–259, 2013.
- [7] Q. Boehler, S. Gervasoni, S. L. Charreyron, C. Chautems, and B. J. Nelson, "On the workspace of electromagnetic navigation systems," *IEEE Transactions on Robotics*, pp. 1–17, 2022.
- [8] Y. Kim, G. A. Parada, S. Liu, and X. Zhao, "Ferromagnetic soft continuum robots," *Science Robotics*, vol. 4, no. 33, p. eaax7329, 2019.
- [9] P. Lloyd, G. Pittiglio, J. H. Chandler, and P. Valdastrì, "Optimal design of soft continuum magnetic robots under follow-the-leader shape forming actuation," in *2020 International Symposium on Medical Robotics (ISMR)*. IEEE, 2020, pp. 111–117.
- [10] H. Ye, Y. Li, and T. Zhang, "Magttice: a lattice model for hard-magnetic soft materials," *Soft Matter*, vol. 17, no. 13, pp. 3560–3568, 2021.
- [11] R. Zhao, Y. Kim, S. A. Chester, P. Sharma, and X. Zhao, "Mechanics of hard-magnetic soft materials," *Journal of the Mechanics and Physics of Solids*, vol. 124, pp. 244–263, 2019.
- [12] R. Dreyfus, Q. Boehler, and B. J. Nelson, "A Simulation Framework for Magnetic Continuum Robots," *IEEE Robotics and Automation Letters*, vol. 7, no. 3, pp. 8370 – 8376, Jun. 2022.
- [13] T. Xu, J. Zhang, M. Salehzadeh, O. Onaizah, and E. Diller, "Millimeter-scale flexible robots with programmable three-dimensional magnetization and motions," *Science Robotics*, vol. 4, no. 29, p. eaav4494, 2019.
- [14] S. Jeon, A. K. Hoshier, K. Kim, S. Lee, E. Kim, S. Lee, J.-y. Kim, B. J. Nelson, H.-J. Cha, B.-J. Yi, and H. Choi, "A magnetically controlled soft microrobot steering a guidewire in a three-dimensional phantom vascular network," *Soft Robotics*, vol. 6, no. 1, pp. 54–68, 2019.
- [15] J. Danczyk and K. Suresh, "Finite element analysis over tangled simplicial meshes: Theory and implementation," *Finite Elements in Analysis and Design*, vol. 70–71, pp. 57–67, 2013.
- [16] "Chapter two - material point method: Overview and challenges ahead," ser. *Advances in Applied Mechanics*, S. P. Bordas and D. S. Balint, Eds. Elsevier, 2021, vol. 54, pp. 113–204.
- [17] Y. Hu, J. Liu, A. Spielberg, J. B. Tenenbaum, W. T. Freeman, J. Wu, D. Rus, and W. Matusik, "Chainqueen: A real-time differentiable physical simulator for soft robotics," 2018. [Online]. Available: <https://arxiv.org/abs/1810.01054>
- [18] F. Sun, G. Wang, L. Zhang, R. Wang, T. Cao, and X. Ouyang, "Material point method for the propagation of multiple branched cracks based on classical fracture mechanics," *Computer Methods in Applied Mechanics and Engineering*, vol. 386, p. 114116, 2021.
- [19] M. Li, Y. Lei, D. Gao, Y. Hu, and X. Zhang, "A novel material point method (mpm) based needle-tissue interaction model," *Computer Methods in Biomechanics and Biomedical Engineering*, vol. 24, no. 12, pp. 1393–1407, 2021.
- [20] Y. Hu, Y. Fang, Z. Ge, Z. Qu, Y. Zhu, A. Pradhana, and C. Jiang, "A moving least squares material point method with displacement discontinuity and two-way rigid body coupling," *ACM Transactions on Graphics*, vol. 37, no. 4, p. 150, 2018.
- [21] C. Jiang, C. Schroeder, J. Teran, A. Stomakhin, and A. Selle, "The material point method for simulating continuum materials." New York, NY, USA: Association for Computing Machinery, 2016. [Online]. Available: <https://doi.org/10.1145/2897826.2927348>
- [22] C. Jiang, C. Schroeder, A. Selle, J. Teran, and A. Stomakhin, "The affine particle-in-cell method," *ACM Transactions on Graphics (TOG)*, vol. 34, no. 4, pp. 1–10, 2015.
- [23] G. Pittiglio, P. Lloyd, T. da Veiga, O. Onaizah, C. Pompili, J. H. Chandler, and P. Valdastrì, "Patient-specific magnetic catheters for atraumatic autonomous endoscopy," *Soft Robotics*, 2022.
- [24] T. Da Veiga, J. H. Chandler, G. Pittiglio, P. Lloyd, M. Holdar, O. Onaizah, A. Alazmani, and P. Valdastrì, "Material characterization for magnetic soft robots," in *2021 IEEE 4th International Conference on Soft Robotics (RoboSoft)*. IEEE, 2021, pp. 335–342.
- [25] A. Shariati, J. Shi, S. Spurgeon, and H. A. Wurdemann, "Dynamic modelling and visco-elastic parameter identification of a fibre-reinforced soft fluidic elastomer manipulator," in *2021 IEEE/RJS International Conference on Intelligent Robots and Systems (IROS)*. IEEE, 2021, pp. 661–667.
- [26] Y. Hu, T.-M. Li, L. Anderson, J. Ragan-Kelley, and F. Durand, "Taichi: A language for high-performance computation on spatially sparse data structures," vol. 38, no. 6, 2019. [Online]. Available: <https://doi.org/10.1145/3355089.3356506>
- [27] Y. Fang, Y. Hu, S.-M. Hu, and C. Jiang, "A temporally adaptive material point method with regional time stepping," *Computer Graphics Forum*, vol. 37, no. 8, pp. 195–204.
- [28] M. Ortner and L. G. Coliado Bandeira, "Magpylib: A free python package for magnetic field computation," *SoftwareX*, 2020.
- [29] W. Hu, G. Z. Lum, M. Mastrangeli, and M. Sitti, "Small-scale soft-bodied robot with multimodal locomotion," *Nature*, vol. 554, no. 7690, pp. 81–85, 2018.